Molecular dynamics simulation of microwave heating of liquid monoethanolamine (MEA): an evaluation of existing force fields

This manuscript was accepted by J. Chem. Phys. Click here to see the version of record. AIP/123-QED

Molecular dynamics simulation of microwave heating of liquid monoethanolamine (MEA): an evaluation of existing force fields

N. D. Afify[1, a)] and M. B. Sweatman[1]

School of Engineering, The University of Edinburgh, The King's Buildings, Sanderson Building, Mayfield Road, Edinburgh EH9 3JL, United Kingdom

(Dated: 17 April 2018)

We present a complete classical molecular dynamics (MD) study of the dielectric heating of liquid monoethanolamine (MEA) at microwave (MW) frequencies ranging from 1.0 to 10.0 GHz. The detailed dielectric properties predicted by a series of existing empirical force fields of MEA were carefully compared to experimental results. We find that all the evaluated force fields were unable to accurately predict experimental static dielectric constant, frequency-dependent dielectric spectra, and MW heating profiles of liquid MEA, although GROMOS-aa is the most accurate of those tested. With an isotropic scaling of partial atomic charges, the modified GROMOS-aa and OPLS-aa force fields could accurately reproduce the experimental static dielectric constant and frequency-dependent dielectric spectra, but they failed to predict MW heating rates directly from MD heating simulations. Thus, the recently presented approach (J. Chem. Theory Comput.11, 683 (2015) and J. Chem. Theory Comput.11, 2792 (2015)) to tune existing force fields is not an ideal approach to produce force fields suitable for accurate dielectric heating studies.

Keywords: Classical molecular dynamics; Empirical force fields of monoethanolamine (MEA); Microwave heating of monoethanolamine (MEA); Dielectric spectra of monoethanolamine (MEA)

[a)]Electronic mail: N.Afify@ed.ac.uk

This manuscript was accepted by J. Chem. Phys. Click here to see the version of record.

I. INTRODUCTION

Dielectric heating of liquids using microwave (MW) radiation (0.3-300 GHz) is becoming an increasingly important research area, where many applications are emerging. For instance, use of MW dielectric heating in a carbon capture process to regenerate the amine solvent could potentially reduce the overall cost of the process[1]. In order to understand the role of MW in this CO_2 capture process, details of the dielectric response of the employed liquids to MW irradiation are required. These details include an accurate determination of static dielectric constant, frequency-dependent dielectric spectra, and heating rates of these liquids at different MW frequencies.

Classical molecular dynamics (MD) is a very powerful atomistic computational technique which is, in principle, able to characterize detailed dielectric properties of liquids though the prediction of static dielectric constants, frequency-dependent dielectric spectra, and dielectric heating profiles. Since the employed force field is the main ingredient of any classical MD study, the accuracy of the obtained dielectric properties is strongly dependent on the quality of the employed force field.

We recently reported on classical MD simulations of the dielectric heating of liquid water using MW radiation at different frequencies[2]. We concluded that the capability of an empirical force field to correctly predict the dielectric response of liquids to MW radiation should be evaluated on the basis of a joint comparison of the predicted and experimental static dielectric constant, frequency-dependent dielectric spectra, and MW heating rates.

In the present computational study, we focus on the dielectric response of liquid monoethanolamine (MEA) to MW radiation at different frequencies. MEA aqueous solutions are widely used in CO_2 capture applications[1]. For example, a 30 % aqueous MEA solution has been utilized in CO_2 capture at an industrial scale[3,4]. For MEA-water solutions containing 70 % water the CO_2 sorption and desorption processes take place at 40^oC and 120^oC respectively, which makes the CO_2 capture process energetically inefficient[5]. The use of pure MEA liquid in CO_2 capture is not feasible because of the high viscosity of the product. However, the temperature required for CO_2 desorption in the case of pure MEA liquid loaded on the surface of nanoporous TiO_2 is as low as 80 ^oC[6,7].

FIG. 1. The molecular geometry of the monoethanolamine (MEA) molecule C_2H_7NO.

In Figure 1 we illustrate the molecular geometry of the MEA molecule. In this paper we care-

This manuscript was accepted by J. Chem. Phys. Click here to see the version of record.

fully evaluate the accuracy of most available empirical force fields of MEA, namely MEAa2007[8], MEAo2007[8], MEAa2015[9], OPLS-aa[10], OPLS-aam[10], GROMOS-aa[11,12], and GROMOS-ua[11,12]. In Table I we summarize the Lennard-Jones parameters ε and σ and partial atomic charges q employed in the different force fields. The full set of bond, bond angle, and dihedral angle constraints employed in each force field are reported in Table 1 of the Supplementary Material.

While MEAa2007[8], MEAo2007[8], MEAa2015[9], OPLS-aa[10], and OPLS-aam[10], GROMOS-aa[11,12] are all-atoms force fields, GROMOS-ua[11,12] is a united-atoms force field, where each CH_2 group is represented by a single site with an equivalent mass. From table I it can be seen that the first four force fields are just modified versions of the original OPLS-aa force fields[10]. It should be mentioned that in the case of the OPLS-aam force field the dihedral angle constraints reported in table 1 of the Supplementary Material were provided to us by the authors of Ref. [10] through personal communications.

II. COMPUTATIONAL DETAILS

Molecular dynamics simulations were carried out using the Large-scale Atomic/ Molecular Massively Parallel Simulator (LAMMPS) code[13]. The computational work was carried out on the Archer and Cirrus High Performance Computing (HPC) clusters available at the Edinburgh Parallel Computing Centre (EPCC) located at the University of Edinburgh.

All molecular dynamics simulations used 512 MEA molecules (i.e. 5632 atoms) in a cubic box. This sample size was decided on the basis of the size-dependence of the different dielectric properties obtained from exploratory simulations. A time step of 1.0 fs was used for all simulations, with periodic boundary conditions (PBC) applied in all directions to mimic infinite liquid samples. Long-range Coulombic interactions were evaluated using the particle-particle/particle-mesh (PPPM) solver[13], using a precision factor of 1×10^{-6} and a real-space cut-off of 12.0 Å. The short-range interaction cut-off was set also to 12.0 Å. For all simulations bonds involving hydrogen atoms were constrained during dynamics using the Shake algorithm[14] to allow for using a time step of 1.0 fs. All simulations, except those specifically noted, were conducted at 298.0 K and 1 atmosphere of pressure. For clarity, in the following subsections we summarize the different MD simulations and post-processing sets.

This manuscript was accepted by J. Chem. Phys. Click here to see the version of record.

TABLE I. Summary of the Lennard-Jones parameters ε and σ and partial atomic charges *q* employed in the MEAa2007[8], MEAo2007[8], MEAa2015[9], OPLS-aa[10], OPLS-aam[10], GROMOS-aa[11,12], and GROMOS-ua[11,12] force fields. The full set of bond, bond angle, and dihedral angle constrains employed in each force fields are reported in Tables 1, 2, and 3 of the Supplementary Material.

	MEAo2007	MEAa2007	MEAa2015	OPLS-aa	OPLS-aam	GROMOS-aa	GROMOS-ua
Partial atomic charges q [e]							
N	-0.9	-0.88	-0.739	-0.9	-0.982	-0.943	-0.943
H(N)	0.36	0.335	0.297	0.36	0.386	0.377	0.377
C(N)	0.06	0.2	-0.113	0.06	0.372	0.236	
H(CN)	0.06	0	0.136	0.06	-0.02	0	
C(O)	0.145	0.25	-0.007	0.145	0.088	0.19	
H(CO)	0.06	0	0.136	0.06	0.01	0.013	
O	-0.683	-0.6	-0.662	-0.683	-0.738	-0.625	-0.625
H(O)	0.418	0.36	0.383	0.418	0.508	0.362	0.362
CH_2(N)							0.236
CH_2(O)							0.216
Lennard-Jones parameters ε [kcal/mol] and σ [Å]							
N-N	0.17	0.17	0.17	0.17078	0.17078	0.07006	0.07006
	3.25	3.25	3.25	3.3	3.3	3.5722	3.5722
O-O	0.2104	0.2104	0.2104	0.17078	0.17078	0.20306	0.20306
	3.0664	3.0664	3.0664	3.12	3.21	2.95484	2.95484
H(N)-H(N)	0.0157	0.0157	0.0157	0	0	0.02829	0
	1.069	1.069	1.069	0	1	2.37341	0
H(C)-H(C)	0.0157	0.0157	0.0157	0.15063(CO) 0.03013(CN)	0.01500(CO) 0.03000(CN)	0	
	2.4714	2.4714	2.4714	2.5	2.5	0	0
H(O)-H(O)	0	0	0	0	0	0	0
	0	0	0	0	1	0	
C-C	0.1094	0.1094	0.1094	0.06624	0.06624	0.0663	
	3.3996	3.3996	3.3996	3.5	3.5	3.58118	
CH_2-CH_2							0.09812
							4.07038

A. Initial equilibration simulations

The first set of MD simulations aimed to generate fully equilibrated liquid samples to feed to the remaining sets of simulations. First, we energy-minimized the geometry of the starting atomistic

configurations prior to the equilibration stage. Samples were then equilibrated at 298.0 K and 1.0 atmospheric pressure for 5 ns. This simulation time comprised NVT simulation for the first 1 ns, then NPT simulation for the next 3 ns, and finally NVT simulation for the last 1 ns. During the NVT simulations the temperature was controlled by the Nosé-Hoover thermostat[15] using a temperature damping factor of 0.1 ps. During the NPT simulations the temperature and pressure were controlled by the MTK[16] (Martyna-Klein-Tuckerman) thermostat and barostat employing temperature and pressure damping factors of 0.1 ps and 1.0 ps respectively.

B. Calculation of static dielectric constants using the Neumann's formula

To determine static dielectric constants using the Neumann's formula[17] we carried out long equilibrium NVT simulations. During these simulations temperature was controlled by the Nosé-Hoover thermostat using a damping factors of 0.1 ps. For each force field a trajectory of 30 ns was collected and the total dipole moment of the system was recorded each 1, 10, and 100 fs. The obtained trajectories were also used to compute the frequency-dependent dielectric spectra, as explained later.

According to Neumann's formula[17] the static dielectric constant is related to the magnitude of fluctuations of the total dipole moment (i.e. $\langle M.M\rangle - \langle M\rangle.\langle M\rangle$) by Equation 1. In this equation k_B, T, V, and ε_∞ represent the Boltzmann constant, system temperature and volume, and high-frequency dielectric constant. Our calculations confirmed that the term $\langle M\rangle.\langle M\rangle$ is negligible. In these calculations an experimental value of the high-frequency dielectric constant ($\varepsilon_\infty = 2.0903$[18,19]) of MEA was used.

$$\varepsilon_o = \varepsilon_\infty + \frac{4\pi}{3k_BTV}(\langle M.M\rangle - \langle M\rangle.\langle M\rangle) \quad (1)$$

In Figure 1 of the Supplementary Material we report the dependence of the dielectric constant calculated using Neumann's formula on the MD simulation length. Results are reported in the case of the GROMOS-aa[11,12] force field as an example, obtained using three different sampling frequencies of the total dipole moment. The cumulative average of the static dielectric constant was calculated by averaging the values in the last 5 ns and taking into account the effect of the sampling interval. In figure 1 of the Supplementary Material the predicted value in the case of the GROMOS-aa[11,12] force field is shown by the dashed line. From this figure it can be concluded that our simulation time was long enough to obtain a converged value of the static dielectric constant.

This manuscript was accepted by J. Chem. Phys. Click here to see the version of record.

C. Calculation of static dielectric constants using the applied-field method

Our second approach for the determination of the static dielectric constant of MEA involves equilibration of the liquid under an externally applied static electric field[20,21]. According to this method the magnitude of the total dipole moment induced by an external static electric field of intensity E is given by Equation 2. In this equation ε, ε_o, and $\langle V \rangle$ represent the predicted static dielectric constant, vacuum permittivity, and average system volume.

$$\langle M \rangle = (\varepsilon - 1)\varepsilon_o \langle V \rangle E \tag{2}$$

To apply this method we carried out a set of equilibrium NVT simulations. In these simulations, an external electric field with strengths ranging from 0.0 to 0.01 V/Å, with a step of 0.001 V/Å, were applied in the x direction. At each field strength MEA liquids were equilibrated for 400 ps. Temperature was controlled by the Nosé-Hoover thermostat[15] using a temperature damping factor of 0.1 ps. The total dipole moment of the simulation box was computed from the final 50 ps.

The above procedure was repeated by applying an external static dielectric field in the y and z directions. The relation between the electric field strength and the induced average total dipole moment was fitted linearly to obtain the static electric constant from the slope according to equation 2. Figure 2 of the Supplementary Material shows an example set of results, reported in the case of the GROMOS-aa force field. The response appears to be in the linear regime.

D. Calculation of frequency-dependent dielectric spectra

The frequency-dependent dielectric spectra of MEA liquid predicted by each force field were calculated using the following procedure. The total dipole moment autocorrelation function was fitted to an exponential decay function to determine the dielectric relaxation time (τ_D). The fitting process was carried out using the GROMACS g_dielectric analysis tool[22]. Figure 3 of the Supplementary Material demonstrates an example of such fitting in the case of the GROMOS-aa force field.

The determined relaxation time τ_D was then used to calculate the real and imaginary parts of the frequency-dependent dielectric spectra using the Debye relaxation model[23] in the frequency range form 0.001 to 500.0 GHz. According to this model the real and imaginary parts of the dielectric spectrum are given by Equations 3 and 4. In these calculations we used an experimental value of

This manuscript was accepted by J. Chem. Phys. Click here to see the version of record.

the high-frequency dielectric constant of MEA liquid ($\varepsilon_\infty = 2.0903$[18,19]).

$$\varepsilon_{Re}(\omega) = \varepsilon_\infty + \frac{\varepsilon_o - \varepsilon_\infty}{1 + \omega^2 \tau_D^2} \tag{3}$$

$$\varepsilon_{Im}(\omega) = \frac{(\varepsilon_o - \varepsilon_\infty)\omega\tau_D}{1 + \omega^2 \tau_D^2} \tag{4}$$

E. Determination of MW heating rates

In this series of MD simulations, we performed non-equilibrium dielectric heating studies of MEA liquid at the following MW frequencies: 1.0, 2.45, 5.8, and 10.0 GHz. This set of simulations utilized the NVE ensemble. At each frequency an external electric field, with cosine waveform, was applied along the x direction with field amplitude set to 0.01 V/Å. Initial testing confirmed that this field strength is within the linear response regime for all evaluated force fields. For each MW frequency twenty complete electric field cycles were simulated. The average system temperature was recorded at each 0.1 ps.

To obtain the rise in temperature due to the presence of the external electric field the following procedure was adopted. First, the temperature trajectory in the absence of an electric field was linearly fitted. The resulting linear behaviour was then subtracted from each temperature trajectory in the presence of an electric field. The resulting curves represent therefore the rise in system temperature due only to the applied external electric fields. These heating curves were linearly fitted and the predicted heating rate at each MW frequency was calculated. The above procedure was independently repeated two times by applying the electric field along the y and z directions. From these three independent heating simulation sets the average heating rates and their standard errors were computed and compared to experiment.

The experimental heating rates were computed as follows. For a microwave heating process in a closed system, assuming there are no chemical reactions or heat losses due to convection and conduction to the surroundings, conservation of energy leads to Equation 5. In this equation ρ, $\frac{dT}{dt}$, and c_p are the simulation box mass density, heating rate, and the specific heat capacity of the material. ω, ε_o, $\varepsilon_{Im}(\omega, T)$, and $|E(\omega)|$ are the MW frequency, vacuum permittivity, imaginary part of dielectric spectrum at the frequency ω, and the root mean square amplitude of the applied external electric field.

This manuscript was accepted by J. Chem. Phys. Click here to see the version of record.

$$\frac{dT}{dt} = \omega\varepsilon_o |E(\omega)|^2 \frac{\varepsilon_{Im}(\omega, T)}{\rho c_p(T)} \tag{5}$$

III. RESULTS AND DISCUSSION

In the following subsections we present and discuss our different sets of results to properly evaluate the ability of existing empirical force fields to reproduce experimental dielectric properties of the MEA liquid at room temperature. The results of our attempt to improve the best of these empirical force fields by simply scaling the partial atomic charges will be also reported. Results for the static dielectric constant of MEA are presented first, followed by the frequency-dependent dielectric spectra. Finally, we present the predicted heating rates for MEA at different MW frequencies. Finally, an overall conclusion will be made based on all the obtained results.

A. Static dielectric constants

In Table II we compare the experimental static dielectric constant ε_0, bulk density ρ, self-diffusion coefficient D, and constant-pressure specific heat C_p of liquid MEA at 298.0 K to the values predicted by the different empirical force fields. To accurately calculate the self-diffusion coefficients and constant-pressure specific heats we included quantum corrections in our classical molecular dynamics simulations through the utilization of a quantum thermal bath[24]. Self-diffusion coefficients were calculated using the Einsteins relation[25] utilizing the mean squared displacement (MSD) recorded from 20 ns NVT simulations. The constant-pressure specific heats were calculated from energy fluctuations during 2 ns NPT simulations[26]. It should be mentioned that the experimental static dielectric constant of liquid MEA at 298.0 K reported in table II is actually the average of several experimental results available in literature[27–34].

At this point we discuss only the static dielectric constant results, however, the remaining properties in table II will be useful when discussing the predicted heating rates results. From table II it is clear that static dielectric constants predicted by Neumann's formula and the applied-field method agree well with each other. Unfortunately, table II reveals that none of the evaluated force fields was able to accurately predict the experimental static dielectric constant of the liquid MEA at 298.0 K. With the exception of the OPLS-aam force field all the evaluated force fields tend to underestimate the static dielectric constant of MEA. Nevertheless, from table II it is clear that the

TABLE II. Comparison between the experimental static dielectric constant ε_o[27–34], bulk density ρ[33], self-diffusion coefficient D[35,36], and constant-pressure specific heat C_p[37] of liquid MEA at 298.0 K to the values predicted by the original and modified empirical force fields. The reported experimental static dielectric constant is the average of several experimental results[27–34].

Force field label	ε_o			ρ [g/cm^3]	D [10^{-10} m^2/s]	C_P [kJ/kg.K]
	Neumann formula	Applied-field method	Average value			
Experiment	32.8 ± 2.1			1.018	11.0	3.2
MEAo2007	16.8 ± 0.2	15.8 ± 1.1	16.3 ± 0.6	1.133 ± 0.006	7.21 ± 0.17	3.64 ± 0.03
MEAa2007	15.3 ± 0.2	14.4 ± 1.4	14.9 ± 0.7	1.110 ± 0.006	13.28 ± 0.26	3.35 ± 0.04
MEAa2015	11.0 ± 0.2	10.2 ± 1.0	10.6 ± 0.5	1.070 ± 0.006	8.28 ± 0.11	3.07 ± 0.01
OPLS-aa	18.2 ± 0.2	18.3 ± 1.2	18.2 ± 0.6	1.052 ± 0.005	5.63 ± 0.08	3.50 ± 0.04
OPLS-aam	74.1 ± 1.4	77.4 ± 1.2	75.8 ± 0.9	0.986 ± 0.006	5.40 ± 0.04	3.41 ± 0.02
GROMOS-aa	26.3 ± 0.4	28.3 ± 1.3	27.3 ± 0.7	1.095 ± 0.007	7.29 ± 0.06	3.18 ± 0.02
GROMOS-ua	20.3 ± 0.3	20.6 ± 1.4	20.5 ± 0.7	0.969 ± 0.006	7.91 ± 0.10	2.51 ± 0.02
GROMOS-aa and OPLS-aa force fields with scaled partial atomic charges						
GROMOS-aa-q1.025	27.5 ± 0.4	26.6 ± 1.1	27.1 ± 0.6	1.110 ± 0.007	6.02 ± 0.03	3.10 ± 0.01
GROMOS-aa-q1.04	28.2 ± 0.4	29.3 ± 0.9	28.8 ± 0.5	1.121 ± 0.007	4.78 ± 0.08	3.05 ± 0.01
GROMOS-aa-q1.05	28.5 ± 0.7	32.2 ± 0.9	30.4 ± 0.6	1.126 ± 0.006	4.56 ± 0.07	3.21 ± 0.03
OPLS-aa-q1.05	23.2 ± 0.4	20.4 ± 0.8	21.8 ± 0.4	1.069 ± 0.004	3.85 ± 0.03	3.58 ± 0.04
OPLS-aa-q1.098	32.8 ± 0.5	31.5 ± 0.6	32.1 ± 0.4	1.081 ± 0.004	2.58 ± 0.04	3.51 ± 0.02

static dielectric constant predicted by the GROMOS-aa (i.e. 27.3±0.7) is the closest to the average experimental value (i.e. 32.8±2.1).

As mentioned above we modified the parameters of the GROMOS-aa and OPLS-aa force fields to improve their ability to reproduce the experimental static dielectric constant of MEA. Our approach was to proportionately scale the partial atomic charges in these force fields with all the remaining force field parameters left unchanged. This method was first presented by Salas et al.[38] to improve force fields for pyridine, dichloromethane, methanol, and 1-ethyl-3-methylimidazolium tetrafluoroborate (EMIM-BF4) at different temperatures and pressures. Luz et al. followed the same approach to obtain an accurate force field for formamide[39].

Our partial atomic charges scaling factors were as follows: 1.025, 1.04, and 1.05 for the GROMOS-aa force field; 1.05 and 1.098 for the OPLS-aa force field. Molecular dynamics simulations using these modified force fields were carried out exactly in the same way as the original force fields. The resulting static dielectric constant, bulk density, self-diffusion coefficient, and

constant-pressure specific heat predicted by these five modified force fields are reported at the bottom of table II.

From this table, it can be seen that the static dielectric constants predicted by the GROMOS-aa-q1.05 (i.e. 30.4±0.6) and the OPLS-aa-q1.098 (i.e. 32.1±0.4) force fields agree well with the experiment (i.e. 32.8±2.1). At this point it is not possible to claim the superior quality of these new force fields since the predicted dielectric spectra and MW heating rates need to be evaluated first. As reported in table II this charge scaling approach produced bulk densities and self-diffusion coefficients that agree less well with experimental results when compared to the original force fields. Furthermore, we will show later that such charge scaling is not an ideal approach for a detailed study of the MW heating of liquids.

B. Frequency-dependent dielectric spectra

(a) (b)

FIG. 2. Real (Figure 2(a)) and imaginary (Figure 2(b)) parts of the frequency-dependent dielectric spectra of liquid MEA at 298.0 K as predicted by the original (solid lines) and modified (dashed lines) empirical force fields compared to their experimental counterpart at 278.0 K[33] (blue squares) and 308.0 K (red dots)[40]. The horizontal black dashed line indicates to the average experimental static dielectric constant of liquid MEA at 298.0 K. The light grey band in this figure indicates the uncertainty on the average value of experimental static dielectric constant.

Now we move on to the ability of the original and tuned empirical force fields to correctly predict the frequency-dependent dielectric spectra of liquid MEA at 298.0 K, particularly in the MW region. In Figure 2 the real (Figure 2(a)) and imaginary (Figure 2(b)) parts of the frequency-dependent dielectric spectra of liquid MEA at 298.0 K as predicted by the original (solid lines) and charge-modified (dashed lines) empirical force fields are compared to their experimental counterparts. Unfortunately, we could not find experimental dielectric spectra collected at 298.0 K. Instead we report in figure 2 the experimental dielectric spectra collected at 278.0 K[33] (blue squares) and 308.0 K (red dots)[40]. The horizontal black dashed line in figure 2(a) indicates the average experimental static dielectric constant of liquid MEA at 298.0 K. The light grey band in this figure indicates the uncertainty on the average value of experimental static dielectric constant as we

considered all the published experimental results[27–34].

Inspection of figure 2 reveals that none of the original force fields (solid lines) are able to reasonably reproduce the real and imaginary parts of the experimental frequency-dependent dielectric spectra of liquid MEA at 298.0 K, which are expected to be located between experimental spectra collected at 278.0 K and 308.0 K. With the exception of the OPLS-aam force field, all the original force fields tend to underestimate the magnitude of the real part and overestimate the frequency location of the main loss peak in the imaginary part of the dielectric spectra. Although, OPLS-aam was the only original force field able to correctly predict the location of the main loss peak in the imaginary part ($\approx$ 1.0 GHz), it tends to overestimate the magnitude of the real part due to the large static dielectric constant predicted by this force field (see table reftab2).

The dielectric spectra predicted by the charge-modified GROMOS-aa and OPLS-aa force fields are reported by the dashed lines in figure 2. From this figure, it can be seen that the real and imaginary parts predicted by the GROMOSaaq1.05 force field (red dashed lines) agree very well with the experimental dielectric spectra collected at 308 K. Additionally, the ability of the OPLS-aa force fields in predicting the experimental dielectric spectra has significantly improved by scaling the atomic partial charges by 9.8 %. However, the dielectric spectra predicted by the OPLS-aa-q1.098 force field (magenta dashed lines) agree better with experimental spectra collected at 278 K. This means that the charge scaling factor for the OPLS-aa force field needed to be smaller than 1.098 to fit better experimental data at room temperature (between the spectra collected at 278 K and 308 K).

C. MW heating rates

As reported and discussed above none of the available empirical force fields for MEA were able to predict either the experimental static dielectric constant nor the experimental frequency-dependent dielectric spectra of liquid MEA at 298.0 K. By scaling the partial atomic charges of some of these force fields we were able to obtain new force fields that are able to predict very well both experimental static dielectric constant and frequency-dependent dielectric spectra of liquid MEA at room temperature. In the following we evaluate the quality of the different force fields for predicting the expected heating rates at different MW frequencies. It will be interesting to see if our modified force fields are also able to correctly describe the heating of liquid MEA by MW radiation at different frequencies.

As explained in section II E our heating simulations are based on simulating liquid MEA with and without the presence of an electric field. As expected from well-equilibrated atomistic configurations, our NVE simulations in the absence of any electric field produced steady temperature profiles which fluctuate around 298.0 K, yet without any significant temperature drift. Then we subtracted these temperature profiles from the ones collected in the presence of electric field at different MW frequencies. Thus, the resulting differential profiles represent the net heating effect due to MW radiation.

In Figure 3 we report the predicted net heating profiles (solid lines) caused by applying external time-dependent electric fields at MW frequencies ranging from 0.0 to 10.0 GHz. In this figure, we report the results obtained using the GROMOS-aa force field as an example. The time duration of each heating profile corresponds to ten full electric field cycles. To clearly visualize the dependence of heating profiles on MW frequency we included in figure 3 the linear fit of each net heating profile (dashed lines). These results demonstrate that our MD simulations were able to detect the heating profile dependence on the applied MW frequency.

FIG. 3. The predicted classical MD net heating profiles of liquid MEA caused by applying an external time-dependent electric field at MW frequencies ranging from 1.0 to 10.0 GHz. Results are reported for the case of the GROMOS-aa force field. The time length of each simulation corresponds to ten full electric field cycles. The dashed lines represent the linear fit of each net heating profile.

Now we evaluate the ability of the different empirical force fields to correctly predict how fast liquid MEA is heated under MW radiation at different frequencies. An accurate force field should be able to accurately capture the correct magnitudes of the heating rates, as well as their dependence on the employed MW frequency. Figure 4 reports a comparison between the experimental (symbols) and classical MD derived MW heating rates of liquid MEA using the original (solid lines in figure 4(a)) and modified (dotted lines in figure 4(b) and solid lines in figure 4(c)) force fields. The error bars reported in figures 4(a) and 4(b) were estimated by repeating the linear fitting of temperature profiles using several simulation time intervals. In this figure two sets of experimental curves are reported. The curve with blue squares correspond to the experimental dielectric spectra collected at 278 K[33] while the curve with red dots correspond to the experimental dielectric spectra collected at 308 K[40]. We did not find any experimental dielectric spectra collected at 298 K in the literature.

(a) (b) (c)

FIG. 4. MW frequency dependence of the experimental (symbols) and predicted heating rates of liquid MEA: (a) calculated from the temperature profiles predicted by the original force fields, (b) calculated from the temperature profiles predicted by the modified force fields, and (c) calculated using equation 5 employing the dielectric spectra, bulk densities, and constant-pressure specific heats predicted by the modified force fields. The two experimental heating rate curves are based on experimental dielectric spectra collected at 278 K (blue squares)[33] and 308 K (red dots)[40]. The employed electric field amplitude is 0.01 V/Åfor all MW frequencies.

The experimental heating rates reported in figure 4 were calculated using equation 5 employing the experimental values of bulk density, constant-pressure specific heat, and the imaginary part of dielectric spectra at each frequency. The predicted MW heating rates reported in figures 4(a) and 4(b) were calculated solely from the temperature profiles resulting from our MD heating simulations, thus no other parameters were used. Finally, the predicted heating rates reported in figure 4(c) were calculated using equation 5 employing the predicted imaginary part of dielectric spectra (figure 2(b)), bulk density and constant-pressure specific heats (table II).

We first discuss the ability of the original force fields to accurately predict heating rates at different MW frequencies. From figure 4(a), it is clear that none of these force fields was able to predict the experimentally expected heating rates. With the exception of the OPLS-aam force field, even the dependence of the predicted heating rate on the applied MW frequency is incorrectly predicted by these original force fields. However, this is expected from figure 2(b) where all the imaginary parts of the predicted dielectric spectra are shifted towards higher frequencies, and thus the heating rates for MW frequencies ranging from 1.0 GHz to 10.0 GHz according to these dielectric spectra should be increasing.

Now we evaluate the heating rates predicted by the modified force fields. From the dotted lines shown in figure 4(b), it is clear that the agreement between experimental and calculated heating rates was slightly improved by scaling the partial atomic charges of the GROMOS-aa force field. In fact, the curve predicted by the GROMOS-aa-q1.05 force field follows the frequency-dependence of the experimental heating rates expected at 308 K. However, this improvement did not occur in the case of the modified OPLS-aa force fields. In fact, the curves predicted by the OPLS-aa-q1.05 and OPLS-aa-q1.098 force fields do not even follow the frequency-dependence of the

experimental heating rates expected at 308 K. This might be explained by the small self-diffusion coefficients and the large constant-pressure specific heats predicted by the OPLS-aa-q1.05 and OPLS-aa-q1.098 force fields (see table II). Nevertheless, it is surprising to obtain such overall poor agreement between experimental and predicted heating rates, which does not reflect the good level of agreement between the experimental and calculated dielectric spectra in the case of the modified force fields (see figure 2(b)).

To evaluate the possibility of presence of any inaccuracies in our heating simulations we computed the MW heating rates predicted by the modified force fields using equation 5. In this equation we used the dielectric spectra , densities, and constant-pressure specific heats predicted by the modified force fields (see table II). The resulting predicted heating rates are compared to the experimental ones in Figure 4(c). From this figure it is clear that the agreement between the experimental and calculated heating rates is much better when we resorted to equation 5 instead of resorting to the temperature profiles predicted by molecular dynamics heating simulations. In fact, both the magnitudes of heating rates and their dependence on the MW frequencies are reproduced better in this figure specially at 1.0 GHz.

Inspection of figure 4(c) reveals that the curve predicted by the OPLS-aa-q1.05 force field agrees better with the experimental curve expected at 308 K while the curve predicted by the GROMOS-aa-q1.05 force field agrees better with experimental curve expected at 278 K. Obviously, better agreements with the experimental heating rates expected at 298 K can be obtained by further tuning of the charges scaling factors for the GROMOS-aa and OPLS-aa force fields. The overall agreement between experimental and predicted curves are now coherent with the agreement between experimental and predicted dielectric spectra curves. From our point of view the poor agreement between experimental and calculated heating rates predicted by our heating simulations is due to a combination of the following two reasons. First, scaling of the partial atomic charges leads to extremely small diffusion coefficients which makes the equilibration of the system under an oscillating electric field very difficult process. Second, our non-equilibrium heating simulations do not include any quantum correction to classical temperatures. Applying such quantum corrections to non-equilibrium classical MD simulations is not yet implemented in the LAMMPS code.

Our results suggest that the use of the charge scaling approach suggested in Refs. 38 and 39 can be useful to tune empirical force fields to correctly predict the static dielectric constants and also frequency-dependent dielectric spectra, but it is unable to provide force fields that are able

inaccurately predict heating profiles and rates based on MD heating simulations. As mentioned above, this is partially caused by the small diffusion coefficients and the large bulk densities induced by increasing the partial atomic charges. Obviously, the best approach would be to refine the existing force fields such that all relevant properties are reasonably predicted. We have carried out several series of additional calculations in an attempt to reach a set of Lennard-Jones parameters (ε and σ) and partial atomic charges (q) such that the experimental static dielectric constant, dielectric spectra, bulk density, and specific heat are reasonably predicted. Unfortunately, this simple isotropic scaling of ε, σ, and q was not successful. It seems that the available force fields need to be reparametrized, however, with more focus on the dielectric properties. In future, we may report on the development of new empirical force fields for MEA aqueous solutions, based on simultaneous fitting against both ab-initio forces and experimental static dielectric constants.

IV. CONCLUSIONS

In summary, we used a comprehensive classical molecular dynamics framework to evaluate the ability of most of the existing empirical force fields for MEA to accurately describe the dielectric response of liquid MEA at room temperature to microwave irradiation at different microwave frequencies. None of the tested force fields was found successful in predicting dielectric properties of liquid MEA.

We tuned some of these force fields by simply scaling their partial atomic charges so that dielectric properties are correctly predicted. Although some of the modified force fields were successful in correctly predicting both the static dielectric constant and frequency-dependent dielectric spectra of liquid MEA at room temperature, they failed in predicting experimental MW heating rates based on molecular dynamics heating simulations. This failure is explained by inaccurate prediction of self-diffusion coefficients, constant-pressure specific heats, and bulk densities, and also by the absence of any quantum correction to our non-equilibrium classical molecular dynamics heating simulations. Thus, it is concluded that whatever approach is followed to improve existing force fields, all the properties relevant to dielectric heating should be carefully considered when optimizing the parameters of these force fields, and that quantum corrections to temperatures should be also included in these heating simulations.

V. SUPPLEMENTARY MATERIAL

See supplementary material for the following extra tables and figures: (1) Summary of bond, bond angle, and dihedral angle constrains employed in the MEAa2007[8], MEAo2007[8], MEAa2015[9], OPLS-aa[10], OPLS-aam[10], GROMOS-aa[11,12], and GROMOS-ua[11,12] force fields, (2) Effect of equilibrium MD simulation length and dipole moment sampling interval on the predicted static dielectric constant of MEA in the case of the GROMOS-aa force field, (3) An example of the linear fit of the relation between the total dipole moment and applied external electric field strength in the case of the GROMOS-aa force field, and (3) An example of the exponential fit of the total dipole moment autocorrelation function of MEA in the case of the GROMOS-aa force field.

ACKNOWLEDGMENTS

We are grateful for funding from the UK Engineering and Physical Sciences Research Council (EPSRC). We would like to thank Prof. X. Fan, Dr. J. Cardona, and Dr. F. Bougie for very useful discussions and comments.

REFERENCES

[1]S. J. McGurk, C. F. Martn, S. Brandani, M. B. Sweatman, and X. Fan, *Appl. Energy* **192**, 126 (2017).

[2]N. D. Afify, and M. B. Sweatman, *J. Chem. Phys.* **148**, 024508 (2018).

[3]M. R. M. Abu-Zahra, L. H. J. Schneiders, J. P. M. Niederer, P. H. M. Feron, and G. F. Versteeg, *Int. J. Greenhouse Control* **1**, 37 (2007).

[4]B. Feng, M. Du, T. J. Dennis, K. Anthony, and M. J. Perumal, *Energy Fuels* **24**, 213 (2010).

[5]J. Tan, H. W. Shao, J. H. Xu, L. Du, and G. S. Luo, *Ind. Eng. Chem. Res.* **50**, 3966 (2011).

[6]Z. Sun, M. Fan, M. Argyle, *Ind. Eng. Chem. Res.* **50**, 11343 (2011).

[7]Z. Sun, M. Fan, M. Argyle, *Energy Fuels* **25**, 2988 (2011).

[8]E. F. da Silva, T. Kuznetsova, B. Kvamme, and K. M. Merz Jr., *J. Phys. Chem. B***111**, 3695 (2007).

[9]G. S. Hwang, H. M. Stowe, E. Paek, and D. Manogaran, *Phys. Chem. Chem. Phys.***17**, 831 (2015).

[10]M. R. Simond, K. Ballerat-Busserolles, J. Y Coxam, and A. A. H. Pdua, *Chem. Phys. Chem.***13,**, 3866 (2012).

[11]N. Schmid, A. P. Eichenberger, A. Choutko, S. Riniker, M. Winger, A. E. Mark, and W. F. van Gunsteren, *Eur. Biophys. J.***40**, 843 (2011).

[12]A. K. Malde, L. Zuo, M. Breeze, M. Stroet, D. Poger, P. C. Nair, C. Oostenbrink A. E. Mark, *J. Chem. Theory Comput.***7**, 4026 (2011).

[13]S. Plimpton, *J. Comput. Phys.***117**, 1 (1995).

[14]J. P. Ryckaert, G. Ciccotti, and H. J. C. Berendsen, *J. Comp. Phys.***23**, 327 (1977).

[15]W. G. Hoover, *Phys. Rev. A***31**, 1695 (1985).

[16]M. E. Tuckerman, J. Alejandre, R. López-Rendón, A. L. Jochim, and G. J. Martyna, *J. Phys. A: Math. Gen.***39**, 5629 (2006).

[17]M. Neumann, and O. Steinhauser, *Chem. Phys. Lett.***102**, 508 (1983).

[18]R. J. Sengwa, V. Khatri, and S. Sankhla, *Proc. Indian Natn. Sci. Acad***74**, 67 (2008).

[19]R. J. Sengwa, V. Khatri, and S. Sankhla, *J. Solution Chem.***38**, 763 (2008).

[20]J. Kolafa, and L. Viererblová, *J. Chem. Theory Comput.***10**, 1468 (2014).

[21]S. Floros, M. Liakopoulou-Kyriakides, K. Karatasos, and G. E. Papadopoulos, *Xu B., ed. PLoS ONE***12**, 1 (2017).

[22]B. Hess, C. Kutzner, D. van der Spoel, and E. Lindahl, *J. Chem. Theory Comput.***4**, 435 (2008).

[23]A. M. Holtzer, *J. Polym. Sci.***13**, 548 (1954).

[24]H. Dammak, Y. Chalopin, M. Laroche, M. Hayoun, and J. Greffet, *Phys. Rev. Lett.***103**, 190601 (2009).

[25]G. Pranami, and M. H. Lamm, *J. Chem. Theory Comput.***11**, 4586 (2015).

[26]A. Rajabpour, F. Y. Akizi, M. M. Heyhat, and K. Gordiz, *Int. Nano Lett.***3**, 2228 (2013).

[27]P. Undre, S. N. Helambe, S. B. Jagdale, P. W. Khirade, S. C. Mehrotra, *J. Mol. Liq.***137**, 147 (2008).

[28]E. IKADA, Y. HIDA, H. OKAMOTO, J. HAGINO, and N. KOIzuM, *Bull. Inst. Chem. Res., Kyoto Univ.***46**, 238 (1968).

[29]M. N. Rodnikova, T. M. Usacheva, I. A. Solonina, and A. B. Razumova, *Russ. J. Phys. Chem. A.***88**, 267 (2014).

[30]C. Caleman, P. J. van Maaren, M. Hong, J. S. Hub, L. T. Costa, and D. van der Spoel, *J. Chem. Theor. Comput.***8**, 61 (2012).

[31]R.C.R. Gaboriaud, *Seances Acad. Sci. Ser. C***264**, 157 (1967).

[32]R. L. Rowley, W. V. Wilding, J. L. Oscarson, Y. Yang, and N. F. Giles, *Data Compilation of Pure Chemical Properties, Design Institute for Physical Properties. AIChE, New York, NY***8**, 61 (2010).

[33]A. V. Patil, and V. P. Pawar, *J. Mol. Liq.***188**, 1 (2013).

[34] *http://www.microkat.gr/msdspd90-99/Ethanolamine.html*.

[35]S. H. I. Ibrahim, and N. R. Kuloor, *Chem. Eng. Sci.***17**, 1087 (1962).

[36]W. J. Thomas, and I. A. Furzer, *Chem. Eng. Sci.***17**, 115 (1962).

[37]P. M. Amundsen, *Calorimetric measurements with CO_2 capture solvents. Master Thesis. Norwegian University of Science and Technology. https://brage.bibsys.no/xmlui/handle/11250/2356126.*, (2015).

[38]F. J. Salas, G. A. Mndez-Maldonado, E. Nez-Rojas, G. E. Aguilar-Pineda, H. Domnguez, and J. Alejandre, *J. Chem. Theory Comput.***11**, 683 (2015).

[39]A. P. de la Luz, G. A. Mndez-Maldonado, E. Nez-Rojas, F. Bresme, and J. Alejandre, *J. Chem. Theory Comput.***11**, 2792 (2015).

[40]A. V. Patil, G. N. Shinde, and V. P. Pawar, *J. Mol. Liq.***168**, 42 (2012).

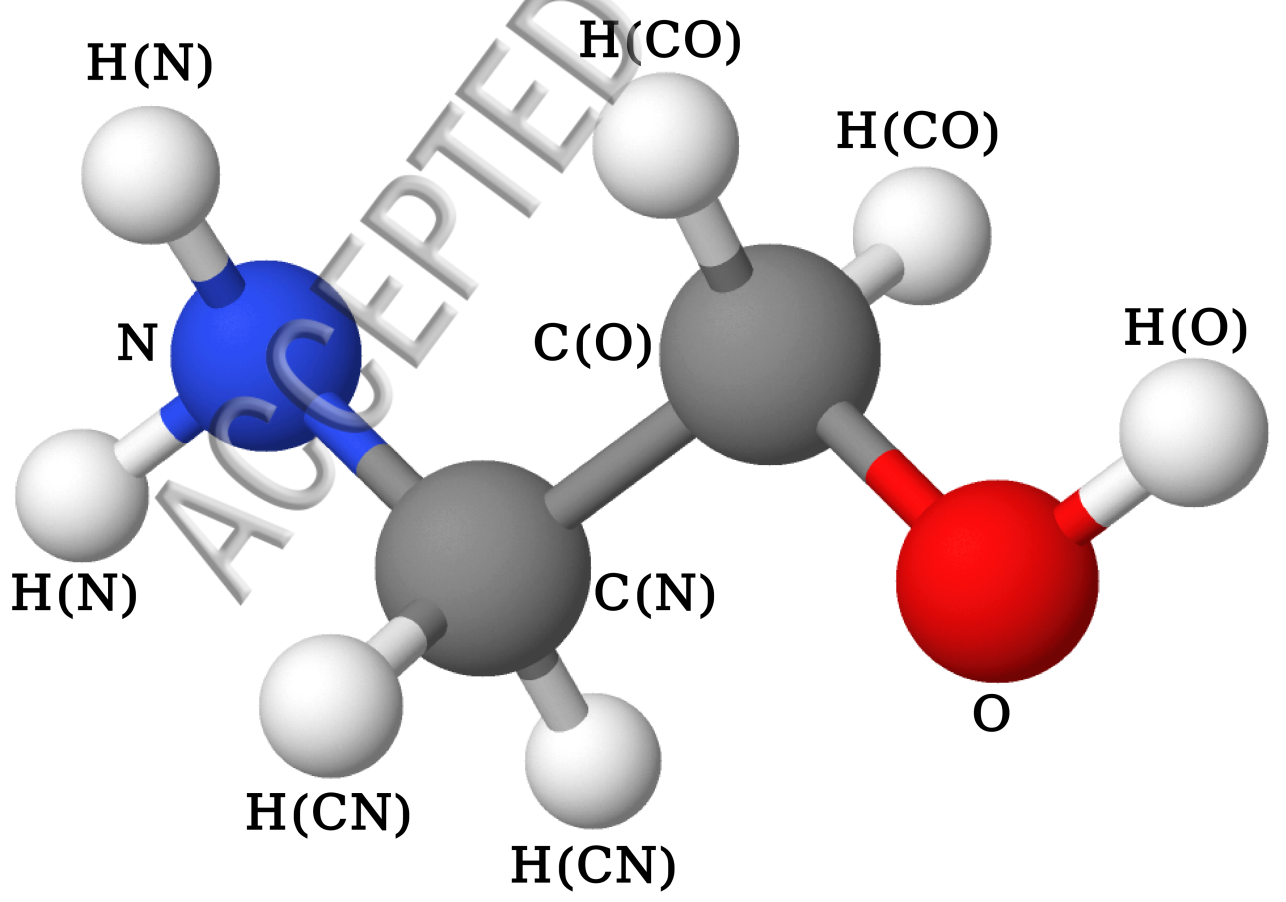

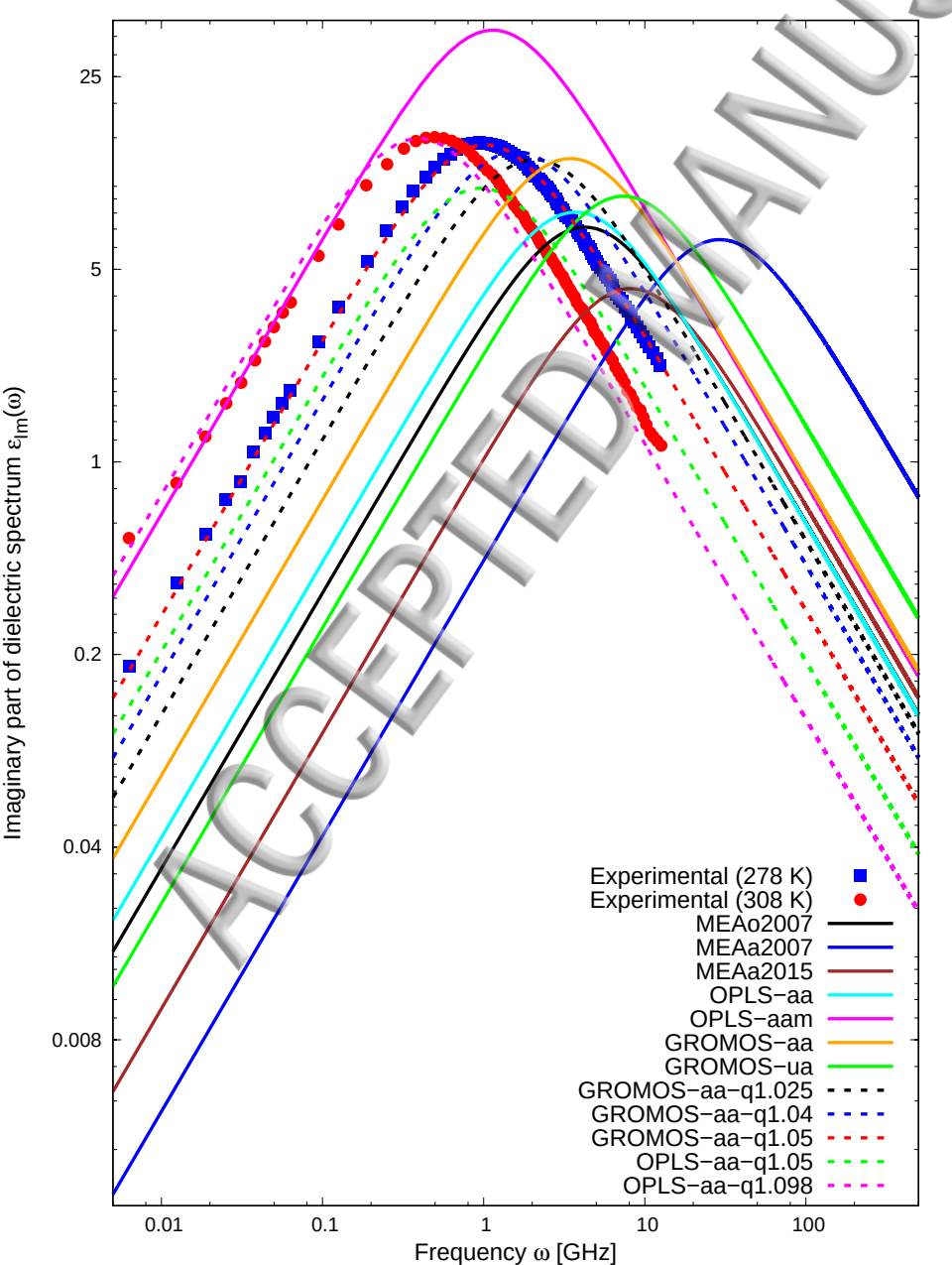

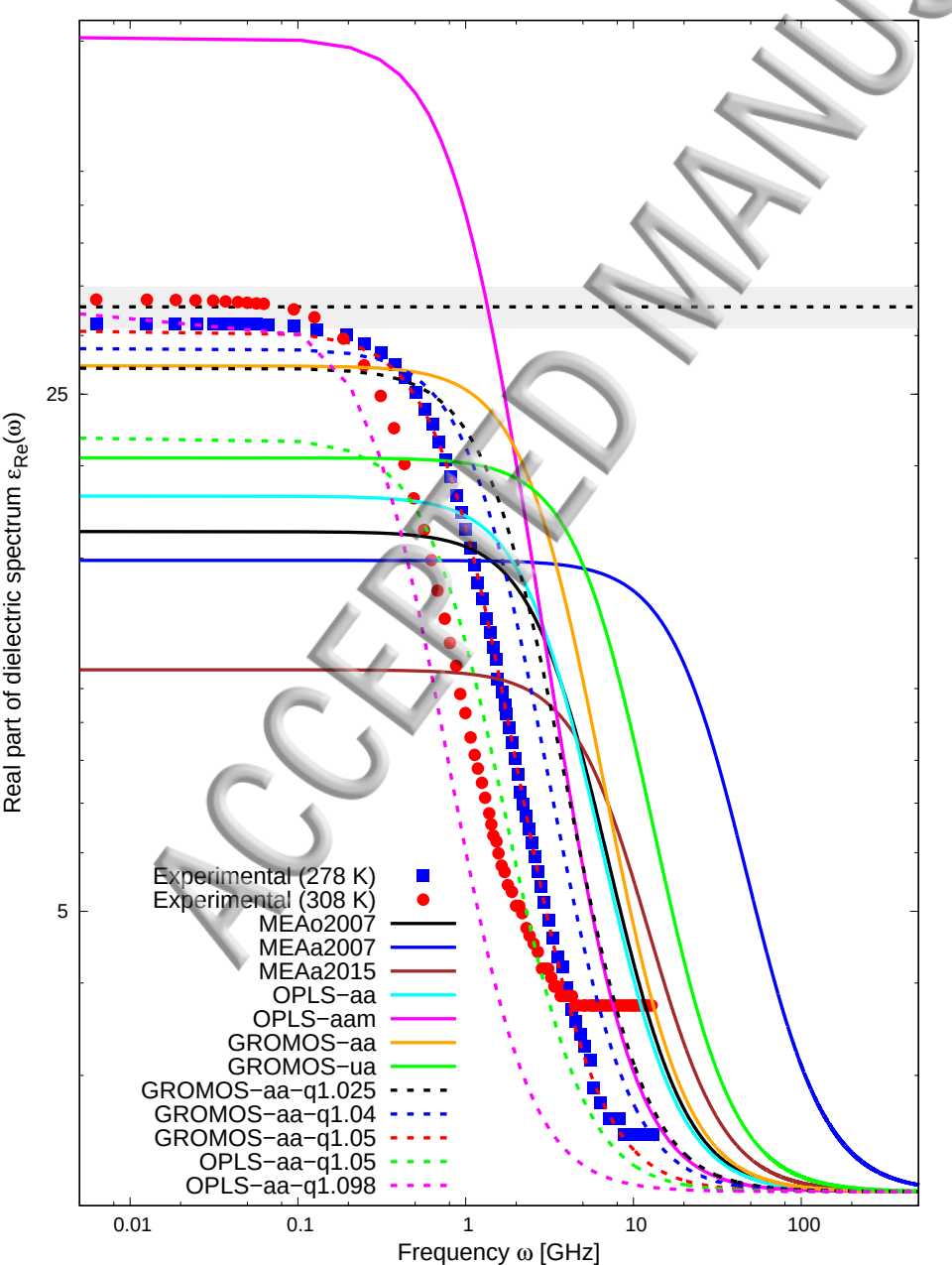

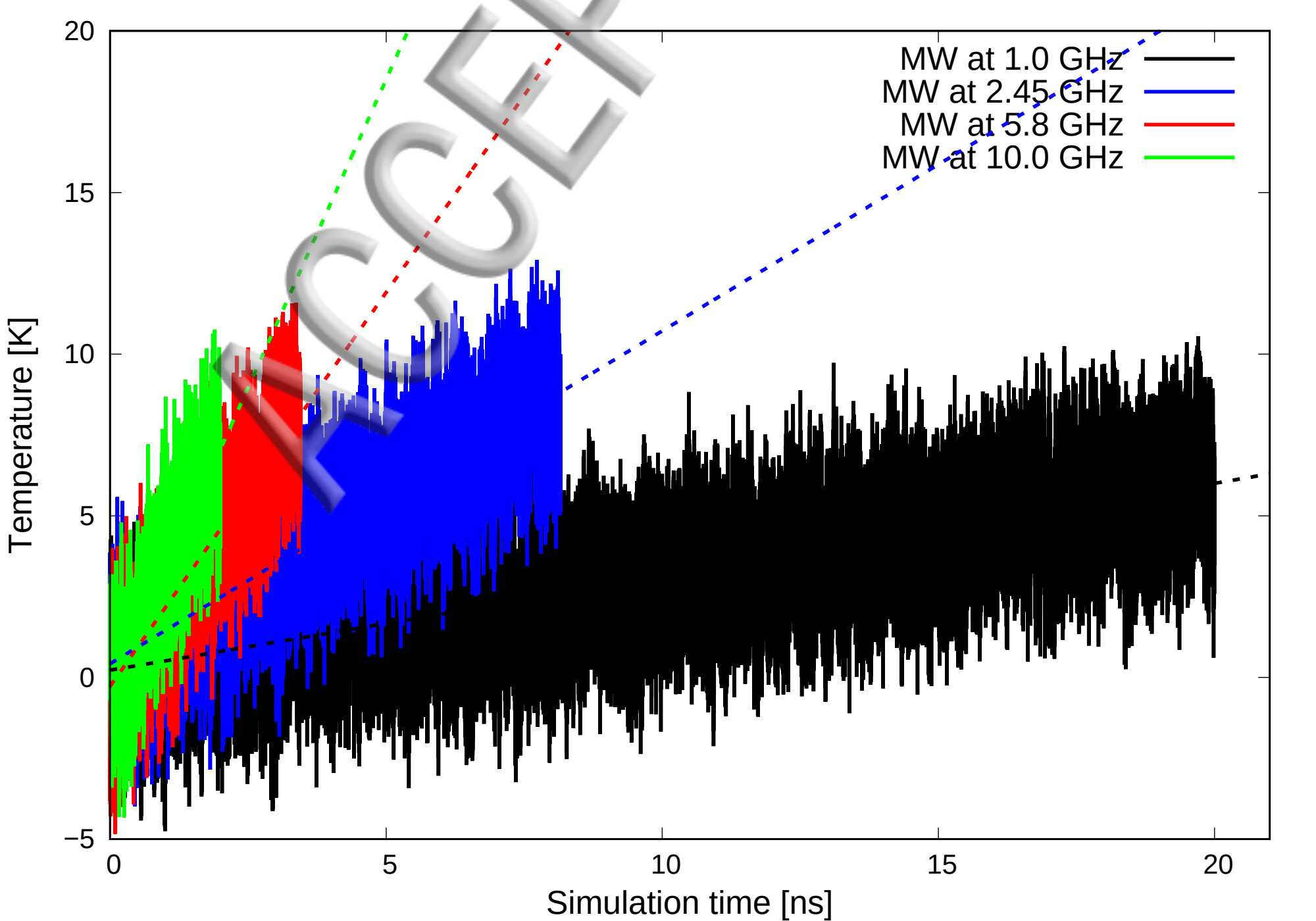
MW at 1.0 GHz
MW at 2.45 GHz
MW at 5.8 GHz
MW at 10.0 GHz
Temperature [K]
Simulation time [ns]
20
15
10
5
0
−5
0
5
10
15
20

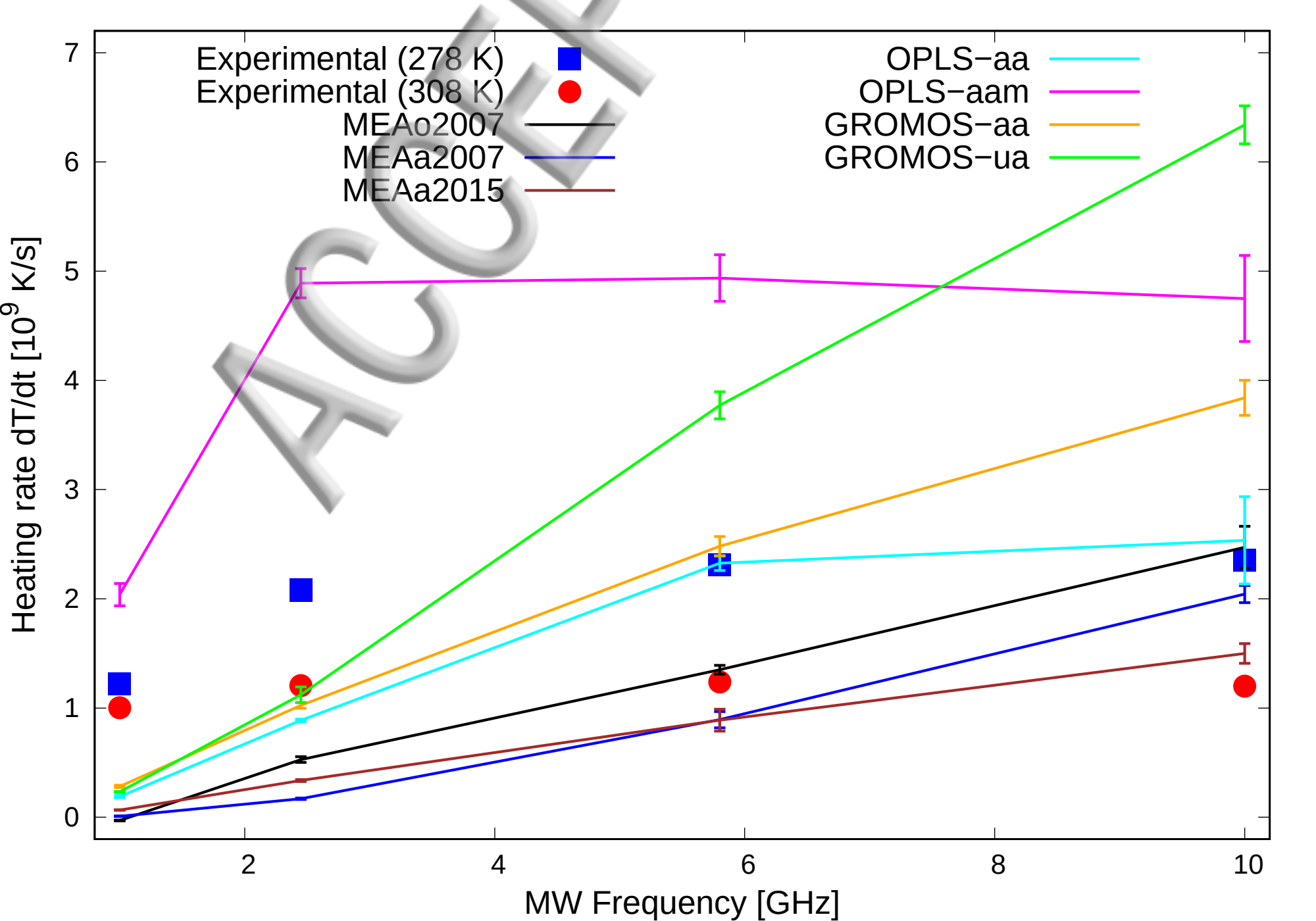
Experimental (278 K)
Experimental (308 K)
MEAo2007
MEAa2007
MEAa2015
OPLS−aa
OPLS−aam
GROMOS−aa
GROMOS−ua
Heating rate dT/dt [10^9 K/s]
MW Frequency [GHz]
0
1
2
3
4
5
6
7
2
4
6
8
10

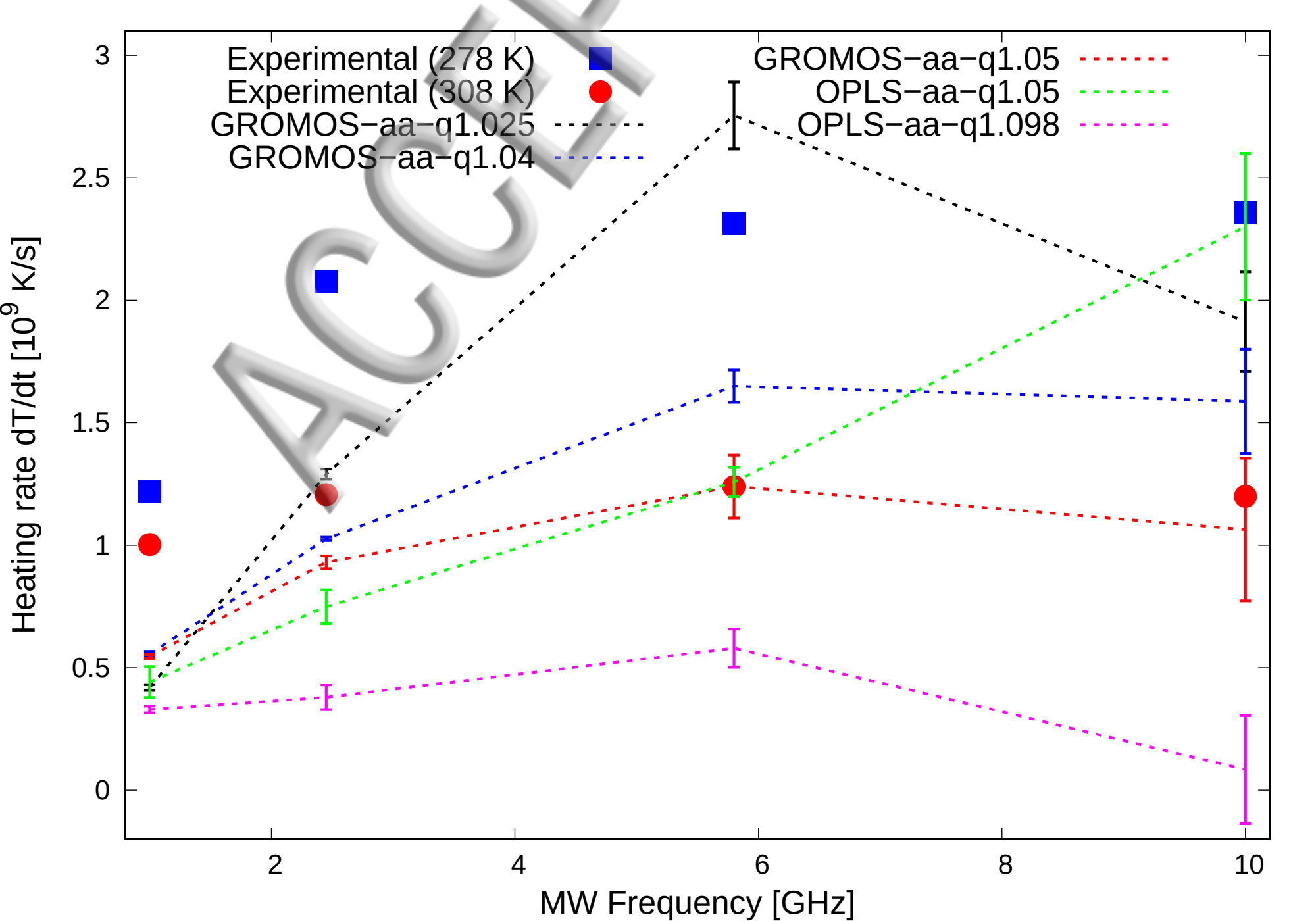
Experimental (278 K)
Experimental (308 K)
GROMOS−aa−q1.025
GROMOS−aa−q1.04
GROMOS−aa−q1.05
OPLS−aa−q1.05
OPLS−aa−q1.098
Heating rate dT/dt [10^9 K/s]
MW Frequency [GHz]
0
0.5
1
1.5
2
2.5
3
2
4
6
8
10

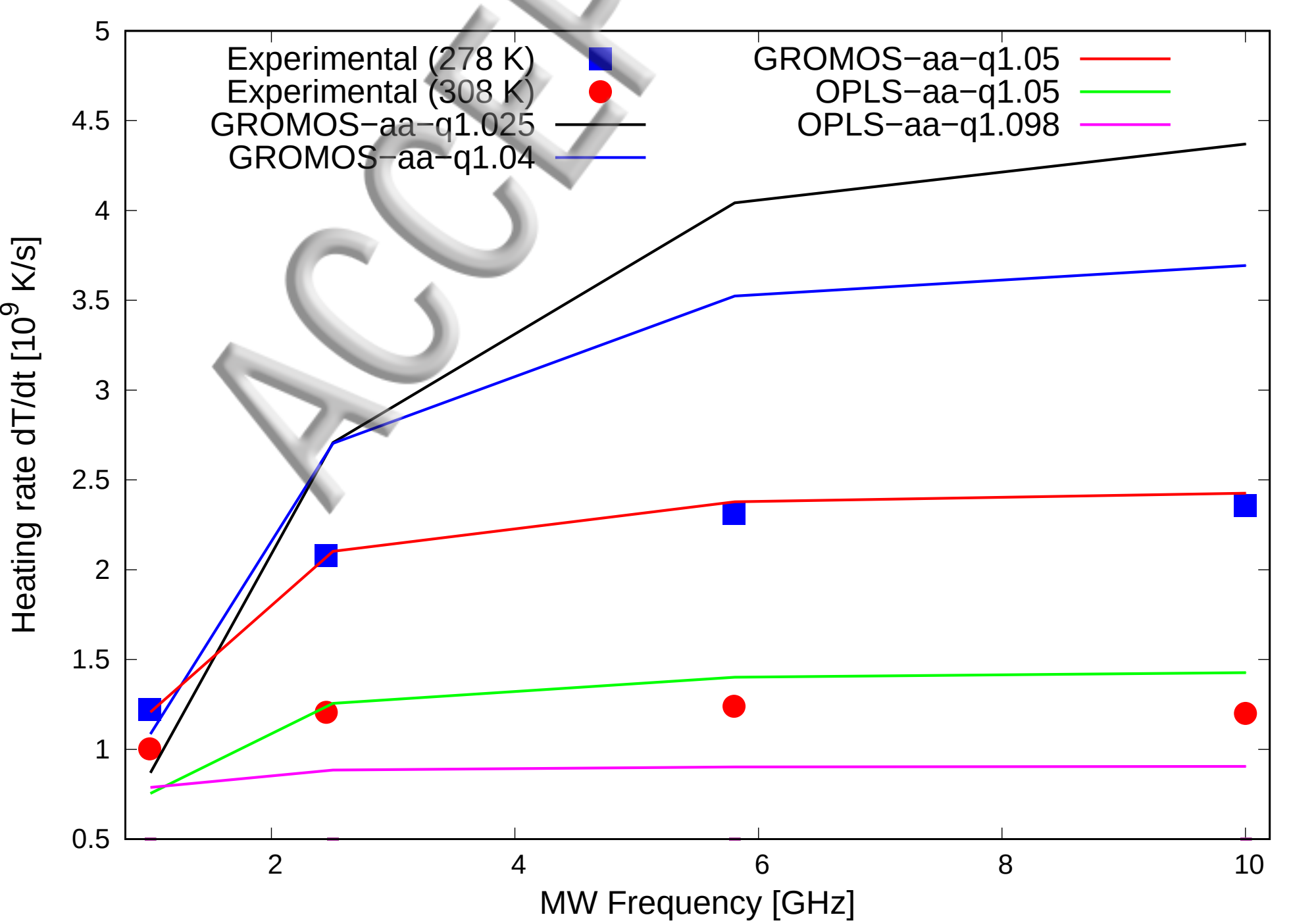
Experimental (278 K)
Experimental (308 K)
GROMOS−aa−q1.025
GROMOS−aa−q1.04
GROMOS−aa−q1.05
OPLS−aa−q1.05
OPLS−aa−q1.098
Heating rate dT/dt [10^9 K/s]
MW Frequency [GHz]
5
4.5
4
3.5
3
2.5
2
1.5
1
0.5
2
4
6
8
10